

Effect of the external fields on the polar and dielectric properties of Eu 0.8 Y 0.2 MnO 3

J. Agostinho Moreira, A. Almeida, W. S. Ferreira, M. R. Chaves, S. M. F. Vilela, P. B. Tavares, B. Kundys, R. Ranjith, and W. Prellier

Citation: *Journal of Applied Physics* **107**, 024108 (2010); doi: 10.1063/1.3291122

View online: <http://dx.doi.org/10.1063/1.3291122>

View Table of Contents: <http://scitation.aip.org/content/aip/journal/jap/107/2?ver=pdfcov>

Published by the [AIP Publishing](#)

Articles you may be interested in

Effect of Pr- and Nd- doping on structural, dielectric, and magnetic properties of multiferroic Bi_{0.8}La_{0.2}Fe_{0.9}Mn_{0.1}O₃

J. Appl. Phys. **115**, 134102 (2014); 10.1063/1.4870454

Dielectric and nonlinear current–voltage characteristics of rare–earth doped CaCu₃Ti₄O₁₂ ceramics

J. Appl. Phys. **110**, 094101 (2011); 10.1063/1.3658258

Grain-boundary effects on magnetotransport properties in La_{2/3}Ca_{1/3}MnO₃/YBa_{1.8}Eu_{0.2}Cu₃O₇ multilayers

J. Appl. Phys. **103**, 07F711 (2008); 10.1063/1.2830629

Magnetic-field-induced switching between ferroelectric phases in orthorhombic-distortion-controlled R MnO₃

J. Appl. Phys. **99**, 08S905 (2006); 10.1063/1.2177207

Effect of YBa₂Cu₃O_{7-δ} film thickness on the dielectric properties of Ba_{0.1}Sr_{0.9}TiO₃ in Ag/Ba_{0.1}Sr_{0.9}TiO₃/YBa₂Cu₃O_{7-δ}/LaAlO₃ multilayer structures

J. Appl. Phys. **97**, 014108 (2005); 10.1063/1.1821644



Not all AFMs are created equal
Asylum Research Cypher™ AFMs
There's no other AFM like Cypher

www.AsylumResearch.com/NoOtherAFMLikeIt

OXFORD
INSTRUMENTS
The Business of Science®

Effect of the external fields on the polar and dielectric properties of $\text{Eu}_{0.8}\text{Y}_{0.2}\text{MnO}_3$

J. Agostinho Moreira,^{1,a)} A. Almeida,¹ W. S. Ferreira,¹ M. R. Chaves,¹ S. M. F. Vilela,² P. B. Tavares,² B. Kundys,³ R. Ranjith,³ and W. Prellier³

¹*Departamento de Física da Faculdade de Ciências, IFIMUP and IN-Institute of Nanoscience and Nanotechnology, Universidade do Porto, Rua do Campo Alegre, 687, 4169-007 Porto, Portugal*

²*Centro de Química, Universidade de Trás-os-Montes e Alto Douro, Apartado 1013, 5001-801 Vila Real, Portugal*

³*Laboratoire CRISMAT, ENSICAEN/CNRS, 6 Boulevard du Maréchal Juin, 1450 Caen Cedex 4, France*

(Received 7 October 2009; accepted 12 December 2009; published online 28 January 2010)

$\text{Eu}_{0.8}\text{Y}_{0.2}\text{MnO}_3$ has been widely studied due to its very distinctive phase diagram, where it is still poorly understood the actual ferroelectric character of the low temperature magnetic phases. In order to figure out what is the origin of the microscopic mechanisms that drive its behavior, we carried out a detailed study of the displacement currents for both different starting conditions and polarizing electric fields, and of the field dependent magnetodielectric effect in $\text{Eu}_{0.8}\text{Y}_{0.2}\text{MnO}_3$ ceramics. The experimental results provide clear evidence for the existence of two dipolar systems, one stemming from an electric field-induced process, likely associated with the isovalent substitution of Eu^{3+} by the smaller off-center Y^{3+} ions at A-lattice sites, which is independent of any cooperative phenomena occurring in the system. The other dipolar system, strongly dependent on the existence of the first one, drives the polar behavior of the nonmodulated magnetic phase AFM-2, stable in the temperature range of 23–30 K, and is associated with the ferroelectric character of this phase. The magnetic field dependence of the complex dielectric constant clearly shows that the magnetodielectric effect is strongly dependent on the phase it is being considered, and provides further evidence for the ferroelectric character of the AFM-2 phase referred to above. © 2010 American Institute of Physics. [doi:10.1063/1.3291122]

I. INTRODUCTION

The control of the electric (magnetic) properties by using magnetic (electric) fields has been an interesting issue of research in both physics and material science for the past decade. The control of the polarization by applying magnetic fields, which is known as the magnetoelectric effect, appears in the materials when the electric polarization and magnetic orders are coupled to each other.¹ It is worth to note that the concept of magnetoelectric effect does not impose any particular magnetic or dipolar structure of the material, where it is observed.¹ In a very special class of materials, called magnetoelectric multiferroics, the magnetoelectric effect can emerge from the coupling between spontaneous polar and magnetic orders of ferroic type, coexisting in the same single phase.^{1–3}

Among the most studied magnetoelectric materials, the undoped perovskite-related rare-earth manganites have drawn a lot of scientific interest due to their rich phase diagrams, which are mainly driven by the rare-earth ionic radius and manganese ion, and their magnetic momentum.⁴ Usually, a detailed analysis of the experimental data is rather complex because it must account for the interplay between the spins of Mn^{3+} and rare-earth ions. Contrarily, the orthorhombic Y-doped EuMnO_3 system exhibits a far more easily magnetic system, wherein its magnetic properties stem only from the

Mn^{3+} ions. So, the changes of its physical properties due to controlled Y-doping cannot be attributed to additional magnetic momenta.

$\text{Eu}_{0.8}\text{Y}_{0.2}\text{MnO}_3$ is one of the most interesting compositions, as it has a very distinctive phase sequence. The paramagnetic phase of $\text{Eu}_{0.8}\text{Y}_{0.2}\text{MnO}_3$ transforms into an antiferromagnetic (AFM-1) phase at $T_N=48$ K, with an incommensurate sinusoidal collinear arrangement of the Mn^{3+} spins.^{5,6} Anomalies in both specific heat and dielectric permittivity evidence another phase transition at $T_{\text{AFM-2}}=30$ K,⁵ where the previous modulated character is completely lost.⁶ Double magnetic-hysteresis loops close to 25 K were reported, revealing the antiferromagnetic character of the phase below $T_{\text{AFM-2}}$, hereafter called AFM-2.⁵ Based on the anomalous behavior of the magnetization curves, a canted antiferromagnetic phase (AFM-3) is established below $T_{\text{AFM-3}}=25$ K.⁵ However, the magnetic structure of the low temperature phases remains unknown, and thus it is still an open question. Based on theoretical arguments, and together with the fact that their data provided evidence for the existence of ferroelectricity below $T_{\text{AFM-2}}$, Hemberger *et al.*⁵ have proposed a noncollinear spiral spin structure between $T_{\text{AFM-2}}$ and $T_{\text{AFM-3}}$, and a conelike structure below $T_{\text{AFM-3}}$.

Contrarily, Yamasaki *et al.*⁶ reported an A-type antiferromagnetic arrangement of the Mn^{3+} spins, occurring from $T_{\text{AFM-2}}$ to the lowest measured temperature, as these authors have not found any evidence of ferroelectricity in $\text{Eu}_{0.8}\text{Y}_{0.2}\text{MnO}_3$.

More recently, a different phase diagram was proposed,

^{a)}Electronic mail: jamoreir@fc.up.pt.

wherein from the two lower magnetic phases, only AFM-2 is actually ferroelectric.⁷ As none of the phases is both ferromagnetic and ferroelectric, it was concluded that this material is not a multiferroic one. A noticeable polarizable character of this compound below $T_{\text{AFM-2}}$ was also reported.⁷

Moreover, a carefully study of the electrically induced magnetization, using a rather low poling electric field (≈ 0.07 kV/cm), evidenced a measurable decreasing of the induced magnetic moment below $T_{\text{AFM-2}}$, reaching a 5% reduction below 10 K.⁷ This result provided a clear evidence for the spin configuration change, due to the poling electric field, which is in good agreement with the existence of a spin-lattice coupling, already found by a previous Raman study in this compound.⁸

In order to gain a better understanding regarding the issues associated with the recently proposed phase sequence of $\text{Eu}_{0.8}\text{Y}_{0.2}\text{MnO}_3$, it is needed to study in more detail the origin and the physical characteristics of the induced polarization occurring in this material. This is a very important aspect as this type of polarization can actually mask any ferroelectric polarization, even when low polarizing electric fields are used, and thus leading to a misinterpretation of the actual phase sequence of this compound.

Though the phase sequence recently proposed in Ref. 7 is clearly supported by the different techniques that were used, experimental evidence obtained from other techniques is still welcome in order to achieve further confirmation of its validity.

In this work, the polar properties of $\text{Eu}_{0.8}\text{Y}_{0.2}\text{MnO}_3$ were studied by measuring the displacement currents in a large temperature range, and under different conditions and applied electric fields. This study is aimed at clarifying the interaction between the different polar mechanisms and the role played by the yttrium ions in this material.

Moreover, the magnetic field dependence of the complex dielectric constant is also presented in order to look for further experimental evidence concerning the occurrence of ferroelectricity at low temperatures.

II. EXPERIMENTAL DETAILS AND MODELING

Most of the experimental work published on $\text{Eu}_{0.8}\text{Y}_{0.2}\text{MnO}_3$ has been performed in single crystals, which has required the processing of high quality crystals, using the floating zone method. Currently, the processing methods for producing polycrystalline samples are much accessible and cheaper, yielding high quality samples. The sol-gel technique has been proved very adequate for processing rare-earth manganites ceramics. In this work, we used ceramic samples, processed through the sol-gel combustion method. The phase purity, the crystallographic and the microstructural characterization of the ceramic samples were checked, by using x-ray powder diffraction and scanning electron microscopy, equipped with energy dispersion spectroscopy. The Rietveld refinement of x-ray diffraction data shows the absence of secondary phases, with occupancy factors converging to the nominal composition of the samples. This result was also confirmed by energy dispersion spectroscopy. Scanning electron microscopy analysis reveals in this system a typical ce-

ramic microstructure with regular shaped crystal grains ranging from 3 to 10 μm in diameter. The mean grain size is about 6 μm . A previous structural, specific heat, dielectric and magnetic characterization of the samples used in this work has, led to results very similar to the ones obtained in single crystals.⁹

The samples used to perform the polar and magnetocapacitive studies have the form of a regular parallelepiped. Gold electrodes were deposited using the evaporation method. The study of displacement currents was carried out in sequential thermal cycles as follows: (i) field cooling-cooling down the sample from room temperature while a polarizing electric field (E) is applied and (ii) zero field heating-heating the sample to room temperature under zero electrical field. The current was measured as a function of temperature, with a standard short-circuit method, using a Keithley electrometer, with 0.5 pA resolution, while keeping a fixed temperature rate. The temperature dependence of the corresponding polarization variation was obtained by the time integration of the current density. The sample temperature was measured with an accuracy better than 0.1 K. In particular, thermally stimulated depolarization currents (TSDC) were analyzed by using the theoretical model presented in Refs. 10–12. According to that model, the dipolar system relaxes obeying a classical Debye model with a single relaxation time, which follows the Arrhenius law. The temperature dependence of the relaxation parameters was found by fitting a straightforward Eq. (1) for $J_{\text{D}}(T)$ presented in Ref. 13, to the experimental data.

The magnetic field dependence of the complex dielectric constant was carried out in a PPMS Quantum Design cryostat, equipped with superconducting coils, generating magnetic fields up to ± 150 kOe. The study of the magnetic field dependence of the dielectric constant at fixed temperature was carried out by using an Agilent 4248A RLC bridge, at different frequencies, in the 10 kHz–1 MHz range.

III. EXPERIMENTAL RESULTS AND DISCUSSION

A. Displacement currents

The study of displacement currents in high-resistive solids can give relevant information about the nature of thermal relaxation processes. Figure 1(a) shows the current density (J_{D}) measured in a heating run, after cooling the samples from 300 to 7 K, at various fixed dc electric fields, using a heating rate of 2 K/min. A broad anomaly at around 110 K, and a more complex one close to $T_{\text{AFM-2}}$ are visible. Hereafter, the high temperature current peak will be called as anomaly I, and the other one as anomaly II. From the Fig. 1(a), it can be noticed that the amplitude of both current anomalies increases with the field strength. Nevertheless, the two anomalies exhibit different electric field and temperature dependences, which enable us to assign each one to different polar mechanisms.

Following Vanderschueren and Gasiot,¹¹ displacement current peaks corresponding to a dipolar relaxation mechanism, are characterized by a field-independent maximum amplitude temperature, and by maximum amplitudes of the current density that are strictly proportional to the field strength.

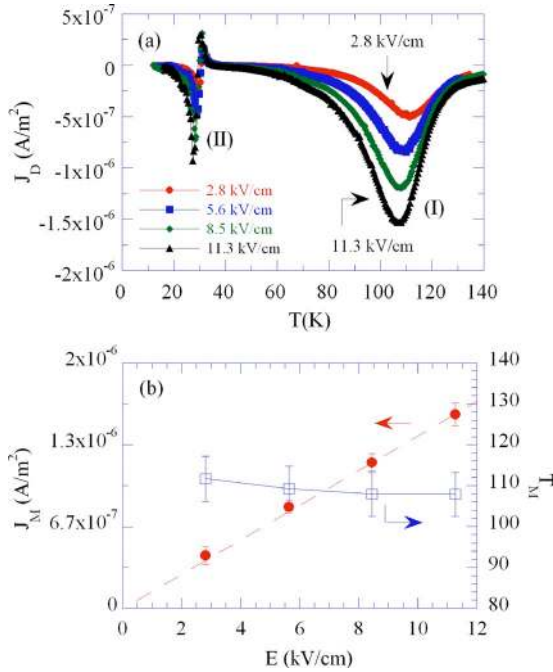


FIG. 1. (Color online) (a) Current density (J_D) measured in a heating run, after cooling the sample from 300 to 7 K, at various fixed dc polarizing electric fields, using a heating rate of 2 K/min. (b) Maximum of the current density (J_M) and the maximum current density temperature (T_M) of anomaly I as a function of the electric field.

Figure 1(b) shows the maximum of the current density (J_M) and the maximum current density temperature (T_M) of anomaly I as a function of the electric field. As it can be seen from Fig. 1(b), $J_M(E)$ is proportional to the electric field up to 11.3 kV/cm, while T_M is nearly constant.

Figure 2 shows $J_D(T)$ measured at various fixed temperature heating rates, after cooling the sample with an applied electric field of 5.6 kV/cm. The shift in anomaly I toward higher temperatures as the heating rate increases, together with the results referred to above, provide a clear evidence for the dipolar relaxation nature of anomaly I. Taking into account the main features of the experimental results obtained, we identify the displacement current measured above 40 K, as field-induced TSDC. Assuming a monodipolar relaxation, we have used the model of Bucci *et al.*¹⁰ to calculate the characteristic parameters of the dipolar relaxation process associated with the anomaly I. The results obtained are depicted in Fig. 3, where we can observe the equilibrium

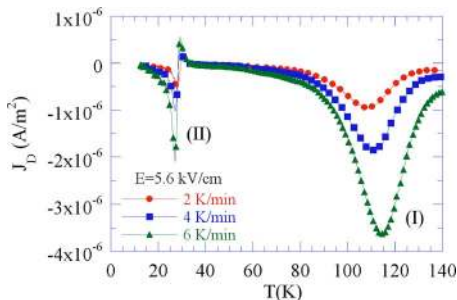


FIG. 2. (Color online) $J_D(T)$ measured at various fixed temperature heating rates, after cooling the sample with a polarizing applied electric field of 5.6 kV/cm.

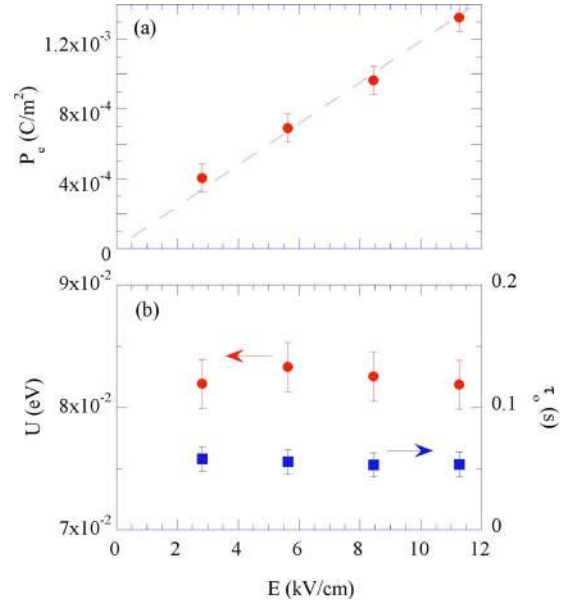


FIG. 3. (Color online) Equilibrium polarization (P_e), activation energy (U), and relaxation time at infinite temperatures (τ_0) concerning the dipolar relaxation, associated with the anomaly I, as a function of the polarizing electric field E .

polarization (P_e), the activation energy (U) and the relaxation time at infinite temperatures (τ_0), concerning the dipolar relaxation, associated with anomaly I, as a function of the polarizing electric field (E). Whereas the equilibrium polarization is a linear function of the electric field, the activation energy and the relaxation time are quite independent on the field strength. The activation energy is about 0.08 eV, and the relaxation time is approximately 5×10^{-2} s. The rather high value obtained for the relaxation time, excludes an electric polarization associated with the deformation of the electronic shells.

The experimental studies carried out have revealed that the shape of both anomalies I and II are strongly dependent on how the electric field is applied. In the previous described results, we have noticed that, when the sample is cooled from room temperature to 7 K under an external electric field, the anomaly II has a complex temperature behavior, exhibiting two peaks with opposite signs, occurring at rather close temperatures, $T' = 29$ K and $T'' = 27$ K, respectively. We have studied the displacement currents applying the electric field in the temperature range between 150 and 40 K, or from 40 down to 7 K, on cooling the sample. Figure 4(a) shows the current density as a function of the temperature, measured in heating run (heating rate 2 K/min) after cooling the sample with an applied electric field of 5.6 kV/cm between 40 and 7 K. Only one peak, corresponding to anomaly II, is observed, and the amplitude of this peak increases about 20% relatively to the maximum value depicted in Fig. 1(a) for anomaly II. There is no trace of thermally stimulated depolarization mechanism above 40 K, revealing that the high temperature dipolar process is not activated by the electric field applied below 40 K. Figure 4(b) shows the current density as a function of the temperature, measured as follows: the sample was cooled from 150 to 40 K, under an applied electric field of 5.6 kV/cm; at 40 K, the field was

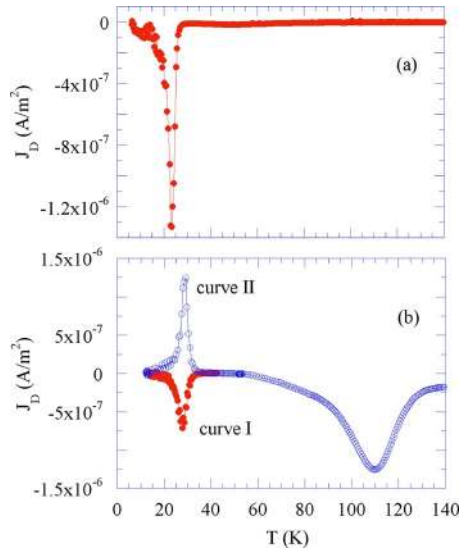


FIG. 4. (Color online) (a) Current density as a function of the temperature, measured in heating run (heating rate 2 K/min) after cooling the sample with a polarizing electric field of 5.6 kV/cm between 40 and 7 K. (b) Current density as a function of the temperature, measured in a cooling run from 40 to 7 K (curve I), and in a heating run from 7 to 150 K (curve II), with a rate of 2 K/min, after cooling the sample from 150 to 40 K, under an electric field of 5.6 kV/cm.

removed and the electrodes short-circuited; then, the current was measured in a cooling run from 40 to 7 K (curve I), and in a heating run from 7 to 150 K (curve II), with a rate of 2 K/min. On cooling, a single peak appears at ~ 28 K, indicating the building up of an electric polarization, even in the absence of an applied electric field in that temperature range. On heating, as expected, the anomaly II changes sign relatively to the previous one, revealing the disappearance of the polarization, and the anomaly I, with opposite sign relatively to the anomaly II, appearing in the same run. The different signs of the two anomalies in this experiment, point out that the two polarizations have opposite directions; i.e., the internal electric field associated with the polarization of anomaly I, determines the orientation of the polarization of anomaly II. These results provide a clear evidence for the strong dependence of the temperature behavior of anomaly II on the depolarizing electric field, generated by the ordered electric dipoles associated with the relaxation process, which gives rise to the anomaly I.

As the anomaly II is strongly dependent on the existence of the field-induced dipolar system, which gives rise the anomaly I, we have studied in detail the electric field dependence of anomaly II, applying the electric field just below 40 K. Then, a detailed study of anomaly II was taken by using different magnitudes for the polarizing electric field in the cooling runs, between 40 and 7 K. Figure 5(a) shows the current density as a function of the temperature, measured in heating run, after cooling the sample with different applied electric fields from 40 down to 10 K. The heating rate was kept fixed at the value of 2 K/min in all measurements. As we can see, only a maximum of the current density occurs at around $T_{AFM-2} = 30$ K. We have calculated the polarization associated with this anomaly by the time integration of the current density. Figures 5(b) and 5(c) show, respectively, the

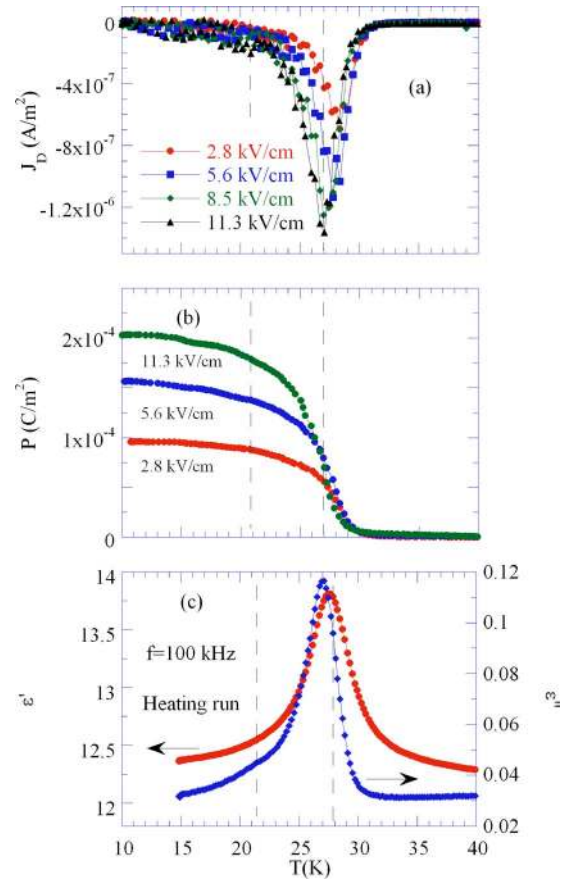


FIG. 5. (Color online) (a) Current density as a function of the temperature, measured in heating run (heating rate 2 K/min), after cooling the sample with different applied electric fields from 40 down to 10 K. (b) Electric polarization obtained from the time integration of the current density presented in (a), for the different polarizing electric fields. (c) The real part (ϵ') and imaginary part (ϵ'') of the dielectric constant at 100 kHz, measured in a heating run.

polarization obtained for the different electric fields, and the real part (ϵ') and imaginary part (ϵ'') of the dielectric constant at 100 kHz, measured in a heating run, for comparison. The electric polarization emerges at $T_{AFM-2} = 30$ K, 3 K above the temperature where the maximum of both $\epsilon'(T)$ and $\epsilon''(T)$ is reached, marking the AFM-1/AFM-2 phase transition. Under an applied electric field of 1 kV/cm, Hemberger *et al.*⁵ have found a polarization of 5×10^{-4} C/m² at 10 K, along the a -axis. In ceramics, due to the random orientation of the ceramic grains, and assuming the proportionality between polarization and applied electric field, the expected mean value of the polarization, for an electric field of 1 kV/cm, is 5×10^{-4} C/m², which is in excellent agreement with the value referred to above. The values of the polarization depicted in Fig. 5(b) are larger than the remanent polarization, reported in a previous work, and calculated from hysteresis loops, measured at 330 mHz, whose maximum value is about 1×10^{-6} C/m².⁷ The comparison of the referred values of both types of polarizations shows clearly that for the magnitude of the polarizing electric field used, already a significant polarization changes below T_{AFM-2} is induced. Moreover, the AFM-2/AFM-3 phase transition it is not revealed by any anomalous behavior of both $J_D(T)$ and $P(T)$. The result presented in Fig. 5(b) corroborates the idea that

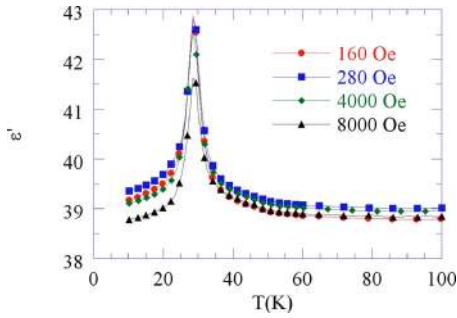


FIG. 6. (Color online) Temperature dependence of the real part (ϵ') of the complex dielectric constant, measured at 100 kHz, for different selected magnetic fields, from 0.16 up to 8 kOe.

the main contribution for the polarization has its origin in an electric induced process, activated by the magnetic ordering rearrangement below T_{AFM-2} .

B. Magnetodielectric effect

Figure 6 shows the temperature dependence of the real part of the dielectric constant (ϵ'), measured at 100 kHz, for different selected magnetic fields, from 0.16 up to 8 kOe. The temperature, where the anomaly of $\epsilon'(T)$ occurs, is apparently independent on the magnetic field strength, and the effect of the magnetic field on the magnitude of the dielectric constant is small, but clearly visible. Nevertheless, the more significant magnetic field-induced changes are observed below T_{AFM-2} , where both polar and magnetic changes have been observed under an electric field.

In order to study in detail the magnetic field effect on the dielectric properties, we have measured the real and imaginary parts of the complex dielectric constant as a function of the magnetic field, up to ± 150 kOe, at 100 kHz, and for several fixed temperatures below 100 K. Figures 7 and 8 show the magnetic field dependence of the real and imaginary parts of the dielectric constant for different fixed temperatures. Above $T_N=48$ K, no significant changes of the ϵ' are induced by the magnetic field [see Fig. 7(f)]. A nonlinear dependence on the magnetic field starts to be observed in the AFM-1 phase, along with a small magnetic-hysteresis. At 30 K, a decrease in the dielectric constant as the magnetic field strength increases is observed just at ± 100 kOe, and then, a further increase in the magnitude of the magnetic field induces an increase in the dielectric constant. Both the shape of $\epsilon'(H)$ and the magnetic-hysteresis change dramatically as the temperature decreases. At 25 K, the maximum magnetic field effect on ϵ' occurs. As the magnetic field increases, ϵ' decreases monotonously in such a way that the two minima, observed at 30 K, are no longer visible. On further cooling, the magnetic field effect decreases, while the field-hysteresis increases. Figure 9 shows the relative field-induced variation in the dielectric constant

$$\frac{\Delta\epsilon}{\epsilon_M} = \frac{\epsilon_M - \epsilon_m}{\epsilon_M} \times 100, \quad (1)$$

which is a quantitative measure of the magnetodielectric effect. In Eq. (1), ϵ_M and ϵ_m denote the maximum and the minimum value of the dielectric constant, respectively. As it

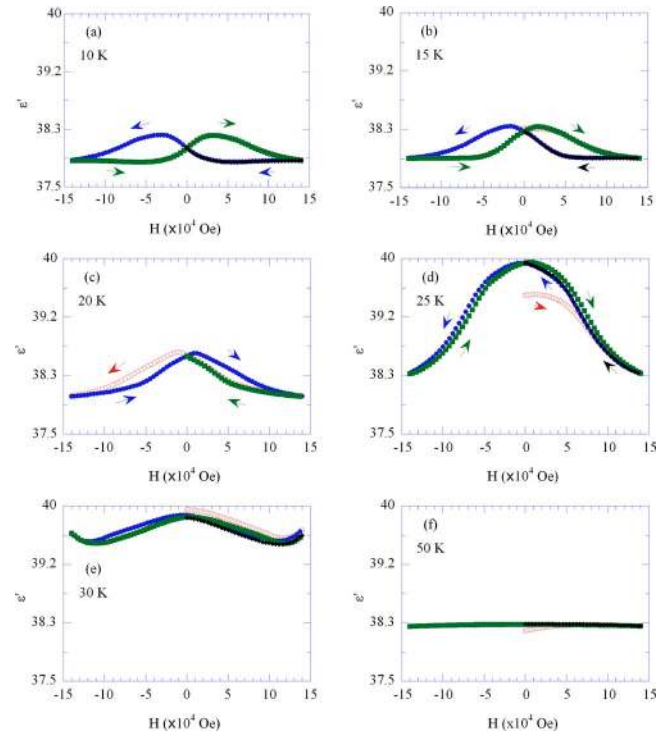


FIG. 7. (Color online) The magnetic field dependence of the real part (ϵ') of the complex dielectric constant for different fixed temperatures.

can be seen in Fig. 9, above $T_N=48$ K, the magnetodielectric effect is negligible small. With decreasing temperature, it starts to increase, reaching the maximum value at around 25 K. On further temperature decrease, a continuously decrease in the magnetodielectric effect is observed.

In Fig. 8 we can see that the magnetic field has not an appreciable effect in ϵ'' in the AFM-1 and in the AFM-3

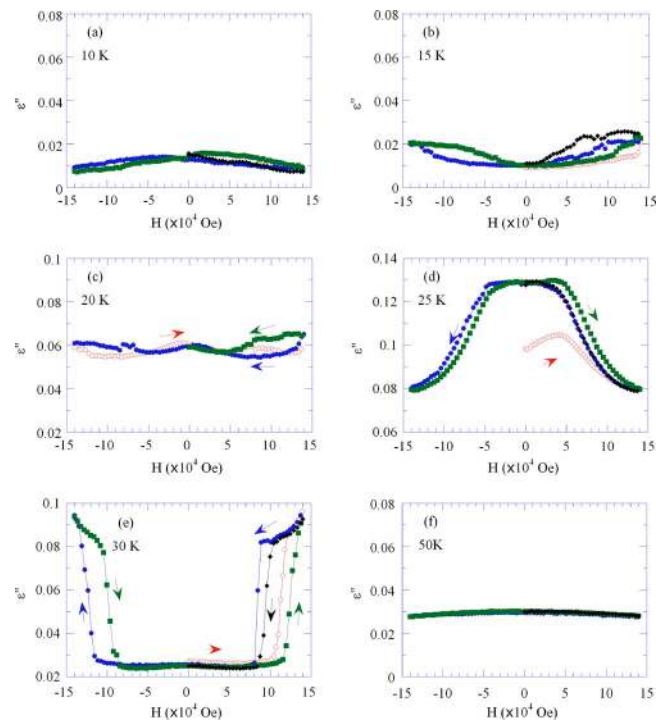


FIG. 8. (Color online) The magnetic field dependence of the imaginary part (ϵ'') of the complex dielectric constant for different fixed temperatures.

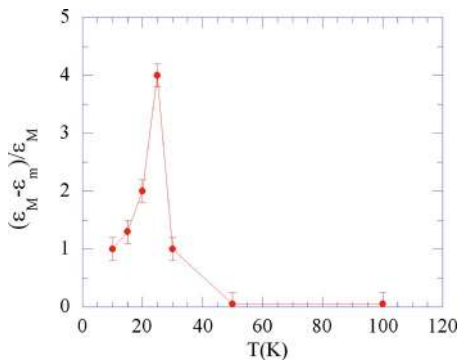


FIG. 9. (Color online) Relative field-induced variation of ϵ' , calculated from Eq. (1).

phases, which are not ferroelectric but has a notorious effect in the AFM-2 phase, which is ferroelectric. As the largest magnetic field-induced changes of the dielectric constant occur in the AFM-2 phase, we can conclude that the magneto-electric coupling is stronger there. From the results displayed in Fig. 8, we have analyzed the temperature dependence of ϵ'' measured at various magnetic field strength, which is presented in Fig. 10, where the magnetic field increases from -150 to 0 kOe. For $H < -100$ kOe, $\epsilon''(T)$ exhibits only a sharp peak, around 25 K. As the magnetic field strength increases from -100 kOe, the peak broadens and its maximum shifts toward higher temperatures.

Finally, it is interesting to stress that for the particular temperature 30 K, a strong magnetic field dependence of $\epsilon''(H)$ and a change in signal of the derivative of $\epsilon'(H)$, are observed at around ± 100 kOe. Therefore, it is plausible that high magnetic fields ($H > 10$ kOe) can induce a phase transition in this compound, near 30 K.

IV. CONCLUSIONS

The study of displacement current performed in a quite large temperature range disclosed two distinct anomalies: one broad anomaly centered at 115 K (anomaly I), and another one, near $T_{\text{AFM-2}}$ (anomaly II). The former is clearly associated with dipolar relaxations leading to relevant induced polarization processes, strongly dependent on the starting conditions and magnitude of the applied polarizing electric field. The source of the dipolar process is most likely associated with the isovalent substitution of Eu^{3+} by the smaller off-center Y^{3+} ions at A-lattice sites. Thus, even low

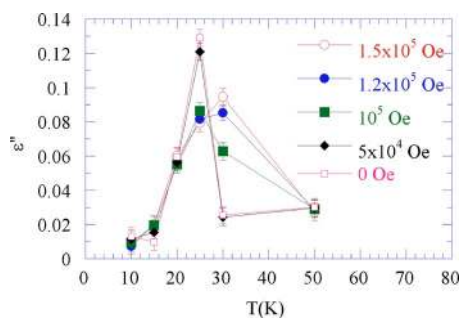


FIG. 10. (Color online) Temperature dependence of ϵ'' measured at various magnetic field strengths. The magnetic field increases from -15 to 0 kOe.

magnitude applied polarizing electric fields can orientate this additional dipolar system, exhibiting its own activation energy and relaxation time, and in this regard, it is completely independent of any cooperative phenomena occurring in $\text{Eu}_{0.8}\text{Y}_{0.2}\text{MnO}_3$. From the fitting of the Bucci–Fieschi model to the experimental data concerning anomaly I, the impurity level was evaluated, yielding an activation energy of ~ 0.08 eV.

Anomaly II is in fact very different from anomaly I. Unlike the latter anomaly, the former one is directly associated with cooperative processes, clearly associated with the AFM-1 to AFM-2 phase transition. Moreover, its amplitude is clearly dependent on the magnitude of the polarizing electric field, providing evidence for its induced polar origin. In order to understand its complex nature, at least two basic mechanisms must be assumed. One mechanism is associated with the magnetic spin arrangement, which couples with phonons, and determines the phase sequence of this material. Another mechanism stems from the strain fields provided by the introduction of Y^{3+} ions into the lattice, thus enhancing the polarizable character of the $\text{Eu}_{1-x}\text{Y}_x\text{MnO}_3$ system, by modifying the spin-phonon interactions. It is worth to note that the induced character of anomaly II may depend on the depolarizing field stemming from the polarization associated with anomaly I, whenever it is induced by adequate polarizing electric fields. In this case, the direction of the polarization yielded at low temperatures is obviously opposite to the direction of the polarization induced at high temperatures.

The polarization obtained from time integration of the displacement currents, measured after applying the electric field below 40 K, is much higher than the magnitude of the remanent polarization, recently reported for ceramic samples.⁷ This result clearly confirms that the major component of the polarization, even for low polarizing electric fields, is of an induced character, revealing the high level of polarizability of $\text{Eu}_{0.8}\text{Y}_{0.2}\text{MnO}_3$.

The magnetic field dependence of the complex dielectric constant clearly shows that the magnetodielectric effect is strongly dependent on the phase it is being considered. The largest effect is observed in the AFM-2 phase, being smaller in the other phases. This result provides further evidence for the ferroelectric character of the AFM-2 phase, which clearly confirms recently published data on the phase sequence of this compound.⁷

The magnetic field dependence of the complex dielectric constant performed at 30 K shows for field above 10 kOe intriguing changes of both its real and imaginary parts. It is likely that they signalize a possible transition into a new phase. Moreover, further studies are still needed in order to confirm this hypothesis.

ACKNOWLEDGMENTS

This work was supported by Fundação para a Ciência e Tecnologia, through the Project No. PTDC/CTM/67575/2006, STREP MACOMUFI and C'NANO Programs, and by Program AlBan, the European Union Program of High Level Scholarship of Latin America (Scholarship No. E06D100894BR).

- ¹W. Eerenstein, N. D. Mathur, and J. F. Scott, *Nature (London)* **442**, 759 (2006).
- ²H. Schmid, *Int. J. Magn.* **4**, 337 (1973).
- ³N. A. Hill, *J. Phys. Chem. B* **104**, 6694 (2000).
- ⁴T. Goto, T. Kimura, G. Lawes, A. P. Ramirez, and Y. Tokura, *Phys. Rev. Lett.* **92**, 257201 (2004).
- ⁵J. Hemberger, F. Schrettle, A. Pimenov, P. Lunkenheimer, V. Yu. Ivanov, A. A. Mukhin, A. M. Blabashov, and A. Loidl, *Phys. Rev. B* **75**, 035118 (2007).
- ⁶Y. Yamasaki, S. Miyasaka, T. Goto, H. Sagayama, T. Arima, and Y. Tokura, *Phys. Rev. B* **76**, 184418 (2007).
- ⁷J. Agostinho Moreira, A. Almeida, W. S. Ferreira, M. R. Chaves, S. M. F. Vilela, and P. B. Tavares, e-print arXiv:0903.5471v1 [cond-mat.mtrl-sci]. (unpublished).
- ⁸J. Agostinho Moreira, A. Almeida, W. S. Ferreira, M. R. Chaves, J. Kreisler, S. M. F. Vilela, and P. B. Tavares, e-print arXiv:0903.4753v1 [cond-mat.mtrl-sci]. (unpublished).
- ⁹J. Agostinho Moreira, A. Almeida, W. S. Ferreira, M. R. Chaves, J. B. Oliveira, J. M. Machado da Silva, M. A. Sá, S. M. F. Vilela, and P. B. Tavares (unpublished).
- ¹⁰C. Bucci, R. Fieschi, and G. Guidi, *Phys. Rev.* **148**, 816 (1966).
- ¹¹J. Vanderschueren and J. Gasiot, in *Thermally Stimulated Relaxation in Solids*, edited by P. Bräunlich, (Springer-Verlag, Berlin, 1979), pp. 135–223.
- ¹²J. Turnhout, in *Electrets*, edited by G. M. Sessler (Springer-Verlag, Berlin, 1980), pp. 81–215.
- ¹³A. Almeida, T. M. Correia, M. R. Chaves, P. M. Vilarinho, A. L. Kholkin, and A. M. Costa, *J. Eur. Ceram. Soc.* **27**, 3701 (2007).